

# Journal of Biomedical Optics

[SPIDigitalLibrary.org/jbo](http://SPIDigitalLibrary.org/jbo)

## **Multifunctional imaging of human retina and choroid with 1050-nm spectral domain optical coherence tomography at 92-kHz line scan rate**

Ruikang K. Wang  
Lin An

# Multifunctional imaging of human retina and choroid with 1050-nm spectral domain optical coherence tomography at 92-kHz line scan rate

Ruikang K. Wang and Lin An

University of Washington, Department of Bioengineering, Seattle, Washington 98195

**Abstract.** The light source at  $\sim 1\text{-}\mu\text{m}$  wavelength is attractive for enhanced imaging depth in retinal optical coherence tomography (OCT). In this paper, we report on a 1050-nm spectral domain OCT system, combined with optical microangiography that operates at a 92-kHz line scan rate for multifunctional imaging of the human eye, delivering the volumetric imaging of microstructure and microvasculature within retina and choroid. © 2011 Society of Photo-Optical Instrumentation Engineers (SPIE). [DOI: 10.1117/1.3582159]

Keywords: retinal optical coherence tomography; spectral domain optical coherence tomography; optical microangiography; one  $\mu\text{m}$  light source.

Paper 11003LRR received Jan. 4, 2011; revised manuscript received Mar. 31, 2011; accepted for publication Apr. 4, 2011; published online May 19, 2011.

Recent development in retinal optical coherence tomography (OCT) has seen considerable interest in the use of 1050 nm ( $\sim 1\ \mu\text{m}$ ) wavelength light source, e.g., Refs. 1–3, in contrast to OCT at 800 nm, because of its ability to significantly increase the choroidal penetration due to the reduced light scattering by retinal pigment epithelium (RPE) layer and its dispersion-free property to the vitreous fluid.<sup>4</sup> The clinical value of imaging choroid by using 1- $\mu\text{m}$  OCT has been demonstrated in patients through its ability to measure the choroidal thickness (ChT) variation over the field of view in uveal inflammation<sup>5</sup> and the vessel density at the center of choroidal neovascularization in age-related macular degeneration.<sup>6</sup> Interest in the choroid also leads to a study in which 3D 1- $\mu\text{m}$  OCT was used to investigate ChT confined to para- and peri-foveal regions.<sup>7</sup> However, these previous studies reported the maximal imaging speed at a 47-kHz line scan rate, which sometimes causes difficulties in patient studies because of the inevitable patient eye and head movements during examination. In addition, there are no studies so far that reported the imaging of microcirculation within retina and choroid by the use of 1- $\mu\text{m}$  light source. In this paper, we report what we believe the first demonstration of the fastest 1- $\mu\text{m}$  spectral domain OCT system combined with the ultrahigh sensitive optical microangiography (OMAG)<sup>8–10</sup> (OCT/OMAG) to achieve multifunctional imaging of microstructures and mi-

crocirculations within retina and choroid, at an unprecedented imaging speed of 92 kHz.

The experimental setup used in this study to achieve 1  $\mu\text{m}$  OCT/OMAG imaging of retinal microstructures and microcirculations is similar to that described in Ref. 10, except for the use of light source and line-scan camera in the system. Briefly, the system employed a 1  $\mu\text{m}$  ASE module (Amonics, ALS-1050-20, China) as the light source, which had a central wavelength of 1050 nm and a bandwidth of 50 nm, delivering  $\sim 10\ \mu\text{m}$  axial resolution in air. The output light from the source was coupled into a 20/80 fiber coupler with 20% light going to the sample arm. In the sample arm, the light was coupled into a custom designed optical probe that consisted of a collimator, an  $x$ - $y$  2D galvanometer scanning system, an objective lens, and an ocular lens to achieve 2D scanning on the posterior segment of the human eye. The estimated lateral resolution was  $\sim 20\ \mu\text{m}$  at the retinal surface. In the reference arm, a  $\sim 20\ \text{mm}$  water cell was used to approximately simulate the vitreous chamber in the human eye. The interferogram between the lights backscattered from the human eye and the reference mirror was recorded by a custom-built high speed spectrometer. An important feature of the spectrometer is the employment of a high speed line scan InGaAs camera with 1024 active elements (SUI, Goodrich Corp, New Jersey) that is capable of providing  $> 80\%$  average detection efficiency around the 1  $\mu\text{m}$  region, and more importantly, delivering an unprecedented line scan rate up to  $\sim 92\ \text{kHz}$ . The designed spectral resolution of the spectrometer was  $\sim 0.11\ \text{nm}$ , providing  $\sim 2.5\ \text{mm}$  detectable depth on both sides of the zero delay line in the air. With the line scan rate of 92 kHz and the sample exposure of  $\sim 2.5\ \text{mW}$ , the measured system sensitivity was  $\sim 105\ \text{dB}$  at the imaging depth of 0.5 mm below the zero delay line, with a  $\sim 20\ \text{dB}$  falling off at the depth of 2.2 mm. For human eye imaging, the system was performed with  $\sim 1.8\ \text{mW}$  of light power at the cornea, well below the maximal power limit for a 10 s exposure.<sup>11</sup> The principle author was the subject for this study.

To show the advantage of the enhanced penetration depth of 1- $\mu\text{m}$  light source, we also used an 800 nm OCT system available in our laboratory<sup>10</sup> to provide results for comparison from the same subject. The parameters used for the 800-nm OCT system were: 850 nm central wavelength, 80-kHz line scan rate,  $\sim 8\ \mu\text{m}$  axial resolution in air, and 110 dB system sensitivity. The results are shown in Fig. 1. Note that in this experiment, we run both the systems at  $\sim 140$  frames per/s (fps), with 512 A scans to cover  $\sim 5\ \text{mm}$  within a B scan on the retina. It is clear that the penetration depth of the 1- $\mu\text{m}$  system is superior to that of the 800-nm system. In the 1  $\mu\text{m}$  OCT tomogram, the retina, choroid, and choroid interface with the sclera are clearly visible with good signal strength [Fig. 1(c)]. In contrast, due to the high scattering and absorption properties of the RPE layer to the 800-nm light, the signals from the choroid and sclera layers were strongly attenuated, making it difficult to interpret the choroid and the interface between the choroid and sclera [Fig. 1(b)]. These observations are similar to those of previous studies where, however, a considerable slower system speed (47 kHz) was used (e.g., Ref. 7).

Next we demonstrate that the 1  $\mu\text{m}$  system, when combined with our unique ultra high sensitive OMAG,<sup>10</sup> is also capable

Address all correspondence to: Ruikang K. Wang, University of Washington, Department of Bioengineering, Seattle, Washington 98195. Tel: 206-616-5025; Fax 206-685-3300; E-mail: wangrk@uw.edu

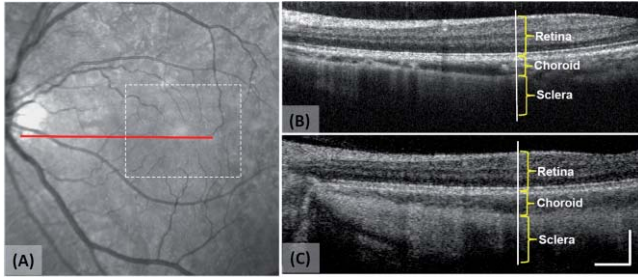


**Fig. 1** Representative B-scan OCT images for comparison between 800 and 1050 nm systems. (a) Standard fundus camera image where the marked red line indicates the approximate position for OCT scanning. The results shown on the right are the OCT tomograms acquired from (b) 800 nm and (c) 1050 nm systems, respectively. White bar = 500  $\mu\text{m}$ .

of visualizing the detailed microcirculation network within the retina and choroid. In this demonstration, we captured 360 A lines to cover  $\sim 3$  mm on each B scan, meaning the space between adjacent A lines was  $< 10$   $\mu\text{m}$ , a minimum requirement in maintaining nominal lateral resolution ( $\sim 20$   $\mu\text{m}$ ) for the system according to the sampling theory. By setting the duty cycle of the  $x$ -scanner (B scanning) at  $\sim 80\%$ , the system was operated at the B-scan imaging rate of 200 fps. For 3D data acquisition, the entire C-scan was evenly divided into 200 steps, with five repeated B-scans in each step. The spacing between the steps was  $\sim 15$   $\mu\text{m}$ . In doing so, it required  $\sim 5$  s to complete one 3D scan (C-scan). Under this scanning protocol, the OMAG algorithm<sup>10</sup> was applied onto the repeated frame sequences at each step. Finally, the 200 calculated B-scan OMAG frames were combined to form one C-scan 3D blood perfusion image of posterior part of the human eye.

Figure 2 gives representative OCT/OMAG B-scan images extracted from one typical C-scan around the macular region of a volunteer, obtained by both the systems used in this study. In the retinal layer, both systems demonstrated abundant capillary flows [e.g., pointed by the open arrows in Figs. 2(c) and 2(d)]. However, the signals from blood vessels deep in the choroidal layer were strongly attenuated [e.g., solid arrows in Fig. 2(c)] for the 800 nm light source. In Fig. 2(d), due to the enhanced penetration depth, the 1  $\mu\text{m}$  system provided strong blood flow signals (e.g., solid arrows) even from deep within the choroidal layer, demonstrating a significant advantage in imaging choroidal blood flows.

Because of the depth-resolved nature, we are able to separate the blood flows in the retina from those in the choroid. In this study, we followed the algorithm described in Ref. 10 to segment depth-resolved flow images from one 3D data set obtained by our 1  $\mu\text{m}$  OCT/OMAG system into six layers. The segmented layers are illustrated in Fig. 2(d). The retinal layer is divided into three layers: R1, R2, and R3, that represent: 1. the radial peripapillary capillaries which locate in the inner part of the retina nerve fiber layer and are the most superficial capillaries of the retina; 2. the inner capillaries that lay in the ganglion cell layers; and 3. the outer capillaries running from the inner plexiform to the outer plexiform layers. We also separated the choroidal layer into three layers: C1, C2, and C3 that represent smaller vessels just below the choriocapillary layer, and medial arterioles and venules and outer arteries and veins, respectively.

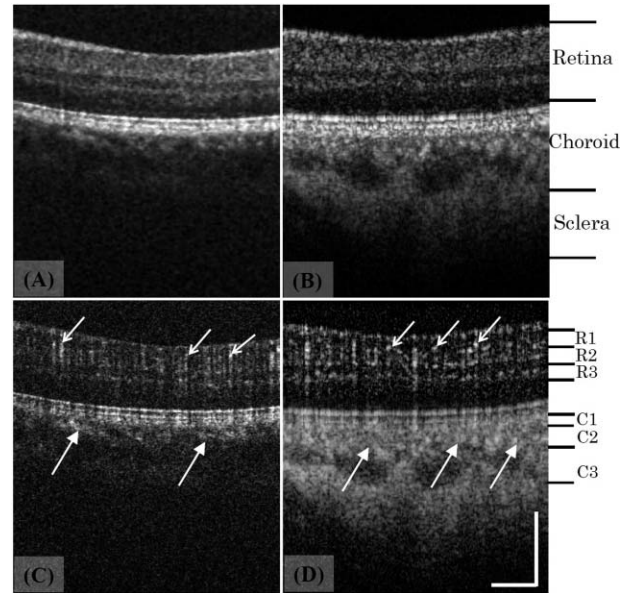


**Fig. 2** (a) Representative B-scan OCT/OMAG images resulting from 800 nm and (b) 1  $\mu\text{m}$  (right) systems, indicating the microstructural images at the top and the blood flow images at the bottom. White bar = 500  $\mu\text{m}$ .

Because the vessels within the thin choriocapillary layer have an average size of  $\sim 5$   $\mu\text{m}$ , which is beyond the capability of current system spatial resolution, we discarded this layer in our segmentation. The segmentation procedure resulted in six volumetric data sets, from which the representative depth-resolved 2D microvascular maps are obtained by the use of maximum amplitude projection. The results are shown in Figs. 3 and 4 for retina and choroid, respectively. It is not surprising that the

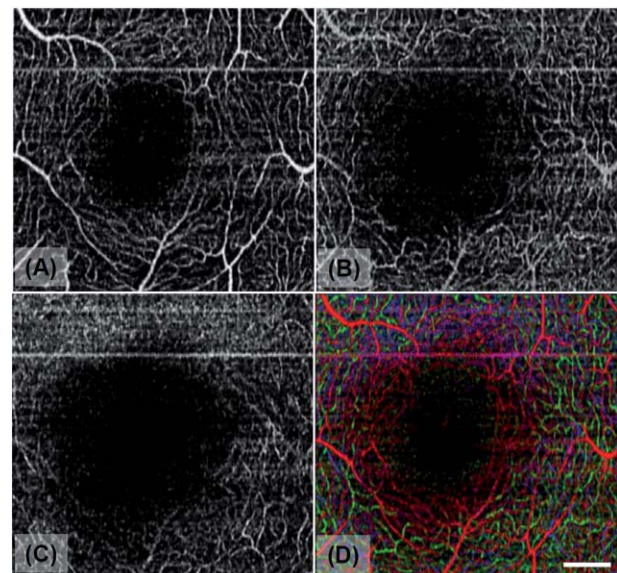


**Fig. 3** Depth resolved retinal blood vessel networks imaged by the 1- $\mu\text{m}$  system from: (a) R1 layer (beyond 425  $\mu\text{m}$  above the RPE layer); (b) R2 layer (between 300 and 425  $\mu\text{m}$  above the RPE layer); (c) R3 layer (between 50 and 300  $\mu\text{m}$  above the RPE layer). (d) Depth encoded color map to appreciate the vasculature located at different depths with red for (a), green for (b) and blue for (c). White bar = 500  $\mu\text{m}$

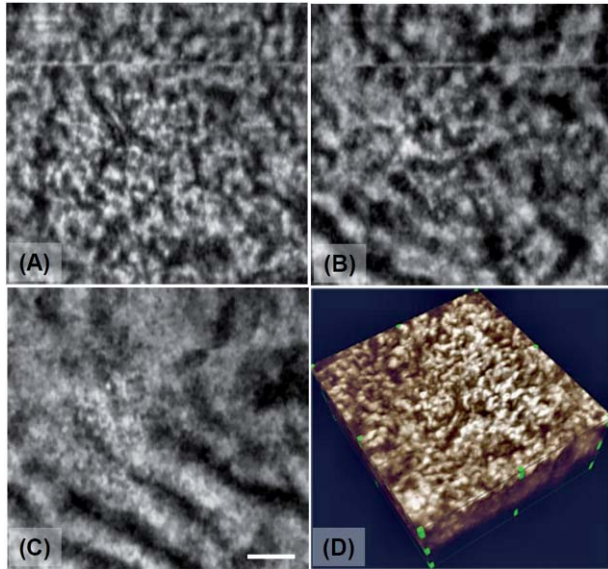


**Fig. 4** Depth resolved choroidal blood perfusion maps from: (a) C1 layer; (b) C2 layer; and (c) C3 layer. (d) 3D visualization of choroidal vasculature. White bar = 500  $\mu\text{m}$ .

retinal capillary networks visualized by the 1- $\mu\text{m}$  system is similar to that of previously reported by using the 800 nm system<sup>10</sup> because the optical signals backscattered from retinal layer does not show a clear advantage for the 1- $\mu\text{m}$  light source over 800 nm. However, because of the deeper penetration depth achieved by the 1  $\mu\text{m}$  light source, clearer visualization of choroidal vessels (C2 and C3) below the choroid capillary layer (C1) can be obtained. Figure 4(d) provides a 3D view of the choroidal vessels. According to the well known Ref. 12, these vessels may be feeding vessels that originate from the big arteries and venues shown in Fig. 4(c) and supply nutrition to the choroidal capillary bed. Further study is needed to confirm these results. Note that the horizontal line in Figs. 3 and 4 was an artifact due to the subject movement.

In conclusion, we have demonstrated the use of a high speed spectral domain OCT/OMAG system (92 kHz line rate) working at the 1- $\mu\text{m}$  wavelength region to provide enhanced penetration depth for imaging of microstructures and microcirculations within human retina and choroid. The demonstrated imaging results offer the depth encoded blood perfusion maps, which cannot be replicated by other technologies such as fluorescent angiography and indocyanine green angiography. The encouraging results promise a great potential for future clinical applications.

This work was supported in part by research from the National Institutes of Health, Grant Nos. R01HL093140, R01EB009682, and R01DC010201. R. K. Wang has a financial interest in OptoVue, Inc. which, however did not support this work.

#### Reference

1. B. Považay, B. Hermann, A. Unterhuber, B. Hofer, H. Sattmann, F. Zeiler, J. E. Morgan, C. Falkner-Radler, C. Glittenberg, S. Blinder, and W. Drexler, "Three-dimensional optical coherence tomography at 1050 nm versus 800 nm in retinal pathologies: enhanced performance and choroidal penetration in cataract patients," *J. Biomed. Opt.* **12**(4), 041211 (2007).
2. A. Unterhuber, B. Považay, B. Hermann, H. Sattmann, A. Chavez-Pirson, and W. Drexler, "In vivo retinal optical coherence tomography at 1040-nm enhanced penetration into the choroid," *Opt. Express* **13**, 3252–3258 (2005).
3. Y. Yasuno, Y. Hong, S. Makita, M. Yamanari, M. Akiba, M. Miura, and T. Yatagai, "In vivo high-contrast imaging of deep posterior eye by 1  $\mu\text{m}$  swept source optical coherence tomography and scattering optical coherence angiography," *Opt. Express* **15**, 6121–6139 (2007).
4. Y. Wang, Z. C. J. Nelson, B. Reiser, R. Chuck, and R. Windeler, "Optimal wavelength for ultrahigh-resolution optical coherence tomography," *Opt. Express* **11**, 1411–1417 (2003).
5. Y. Yasuno, F. Okamoto, K. Kawana, T. Yatagai, and T. Oshika, "Investigation of multifocal choroiditis with panuveitis by three-dimensional high-penetration optical coherence tomography," *J. Biophotonics* **2**, 435–441 (2009).
6. D. M. de Bruin, D. L. Burnes, J. Loewenstein, Y. Chen, S. Chang, T. C. Chen, D. D. Esmaili, and J. F. de Boer, "In vivo three-dimensional imaging of neovascular age-related macular degeneration using optical frequency domain imaging at 1050 nm," *Invest Ophthalmol Vis Sci.* **49**, 4545–4552 (2008).
7. M. Esmaeelpour, B. Považay, B. Hermann, B. Hofer, V. Kajić, K. Kapoor, N. J. L. Sheen, R. V. North, and W. Drexler, "Three-dimensional 1060-nm OCT: choroidal thickness maps in normal subjects and improved posterior segment visualization in cataract patients," *Invest. Ophthalmol. Vis. Sci.* **51**, 5260–5266 (2010).
8. R. S. Wang, S. Jacques, Z. Ma, S. Hurst, S. Hanson, and A. Gruber, "Three dimensional optical angiography," *Opt. Express* **15**, 4083–4097 (2007).
9. R. K. Wang, L. An, S. Saunders, and D. Wilson, "Optical microangiography provides depth resolved images of directional ocular blood perfusion in posterior eye segment," *J. Biomed. Opt.* **15**, 020502 (2010).
10. R. K. Wang, L. An, P. Francis, and D. Wilson, "Depth-resolved imaging of capillary networks in retina and choroid using ultrahigh sensitive optical microangiography," *Opt. Lett.* **35**, 1467–1469 (2010).
11. American National Standard Institute, "Safe use of lasers and safe use of optical fiber communications," New York: ANSI, Z136 committee; 2000:168.
12. P. Henkind, R. I. Hansen, and J. Szalay, "Ocular circulation," in *Physiology of the Human Eye and Visual System*, R. E. Records, Ed., pp. 98–155, Harper & Row, New York (1979).